

Geophysical Research Letters*



RESEARCH LETTER

10.1029/2025GL117713

Key Points:

- Relative variations in fault slip rate along surface traces of normal faults can be estimated from the dip angle of mountain-front facets
- Absolute slip rates can be quantified by combining facet erosion rates derived from cosmogenic nuclides with measurements of facet angle
- Application of facet-angle analysis to the Wasatch fault zone provides further evidence that slip rates have accelerated in the Holocene

Supporting Information:

Supporting Information may be found in the online version of this article.

Correspondence to:

S. W. McCoy, scottmccoy@unr.edu

Citation:

Struble, W. T., McCoy, S. W., Tucker, G. E., Hobley, D. E. J., Gregory, L. C., & Mason, H. B. (2025). Dip angles of mountain-front facets encode long-term slip rates along the Wasatch normal fault, USA. *Geophysical Research Letters*, 52, e2025GL117713. https://doi.org/10.1029/2025GL117713

Received 24 JUN 2025 Accepted 10 NOV 2025

Author Contributions:

Conceptualization: William T. Struble, Scott W. McCoy, Gregory E. Tucker Data curation: William T. Struble, Scott W. McCoy

Formal analysis: William T. Struble, Scott W. McCoy, Laura C. Gregory Funding acquisition: Scott W. McCoy, Gregory E. Tucker, Daniel E. J. Hobley Investigation: William T. Struble, Scott W. McCoy, Gregory E. Tucker, Daniel E. J. Hobley

Methodology: William T. Struble, Scott W. McCoy, Gregory E. Tucker Project administration: Scott W. McCoy

© 2025. The Author(s).

This is an open access article under the terms of the Creative Commons Attribution-NonCommercial-NoDerivs License, which permits use and distribution in any medium, provided the original work is properly cited, the use is non-commercial and no modifications or adaptations are made.

Dip Angles of Mountain-Front Facets Encode Long-Term Slip Rates Along the Wasatch Normal Fault, USA

William T. Struble¹, Scott W. McCoy², Gregory E. Tucker³, Daniel E. J. Hobley³, Laura C. Gregory⁴, and Henry B. Mason²

¹Department of Earth and Atmospheric Sciences, University of Houston, Houston, TX, USA, ²Department of Geological Sciences and Engineering, University of Nevada, Reno, NV, USA, ³Cooperative Institute for Research in Environmental Sciences (CIRES) and Department of Geological Sciences, University of Colorado, Boulder, CO, USA, ⁴School of Earth and Environment, University of Leeds, Leeds, UK

Abstract Mountains bounded by seismogenic normal faults are commonly decorated with facet slopes: planar slopes made of bedrock, or bedrock mantled by regolith, that rise above the fault. The steepness of such slopes is thought to reflect a balance between fault slip and erosion rate. We show that facet dip angles along the Wasatch fault zone (WFZ), USA, positively correlate with fault slip rates, such that relative variations in slip rate can be estimated from facet angle, and that by constraining millennial-scale facet erosion rates, absolute slip rates can be estimated. We calculate ~ 100 -ka average vertical slip rates of $0.37^{+0.36}_{-0.1}$ mm/yr (mean and 90% confidence interval) along the central WFZ, consistent with estimates from features offset over similar timescales, but lower than Holocene rates. Our results provide evidence of slip rate acceleration on the WFZ, and demonstrate the potential of facet-angle analysis to estimate slip rates on range-bounding normal faults.

Plain Language Summary When geologists surveyed the western United States in the 1800s, they were intrigued by facet slopes: planar slopes that rise from the toe of a mountain range and face the adjacent basin flats. They thought these slopes might provide clues to the existence of an earthquake fault. As population increased in Salt Lake City, at the base of Utah's Wasatch Mountains, the question arose: What is the hazard of earthquakes on the faults along which the mountains rise? To help answer this question we develop a method to assess fault activity based on the steepness of facet slopes. According to a geometric model, by combining measurements of facet slope angle and facet erosion rate, it should be possible to obtain an estimate of the rate of fault motion averaged over many earthquakes. We tested this idea along the Wasatch fault zone, an approximately 220-mile-long series of faults in central Utah. The resulting estimates of slip rate are consistent with independent estimates averaged over approximately 100,000 years. This agreement of rates is significant because it suggests that measurements of facet steepness can be used as a reconnaissance tool to estimate potential earthquake activity directly from the shape of mountain fronts.

1. Introduction

Earthquake hazard relates to the rate at which tectonic strain accumulates and is released in earthquakes (Petersen et al., 2015; Woessner et al., 2015). Extrapolation of the historical and instrumental record of seismicity, which may cover only a short portion of the earthquake cycle, can underestimate earthquake rates for the largest earthquakes along a fault (Schwartz & Coppersmith, 1984; Wesnousky, 1994). Long-term fault slip rates can provide independent constraints on the return times of the largest earthquakes or provide geologic constraints to fault deformation models, as explicit rates or categorical proxies, and are therefore key components of earthquake-hazard forecasts (Anderson & Biasi, 2016; Field et al., 2025; Hatem, Reitman, et al., 2022; Petersen et al., 2015; Schwartz & Coppersmith, 1984; Wesnousky, 1994; Woessner et al., 2015; Wong et al., 2016). Unfortunately, well-justified long-term slip-rate estimates are difficult to obtain. Paleoseismic trenching is a developed method to constrain earthquake timing and recurrence rates, but slip rates from this methodology generally have large uncertainty, particularly for sparsely sampled or slowly slipping faults for which there are few to no events in recent geologic time (McCalpin, 2009). Detailed studies dating offset geologic or geomorphic markers can provide more direct estimates of slip rate averaged over thousands of years (e.g., Koehler & Wesnousky, 2011; Wesnousky et al., 2005); however, preservation of offset landforms such as fans, terraces, moraines, or shorelines commonly used to constrain rates over 10–100 ka can be poor (McCalpin, 2009). These challenges limit the collection of slip-rate histories that span multiple earthquake cycles and have sufficiently

STRUBLE ET AL. 1 of 13

19448007, 2025, 22, Downloaded from https://agupubs.onlinelibrary.wiley.com/doi/10.1029/2025GL117713 by University Of Leeds Brotherton, Wiley Online Library on [25/11/2025]. See the Terms and Conditions

Resources: Scott W. McCoy Software: William T. Struble, Scott W. McCoy, Gregory E. Tucker Supervision: Scott W. McCoy Validation: William T. Struble, Scott W. McCoy, Henry B. Mason Visualization: William T. Struble, Scott W. McCoy

Writing – original draft: William T. Struble, Scott W. McCoy Writing – review & editing: William T. Struble, Scott W. McCoy, Gregory E. Tucker, Daniel E. J. Hobley, Laura C. Gregory, Henry B. Mason

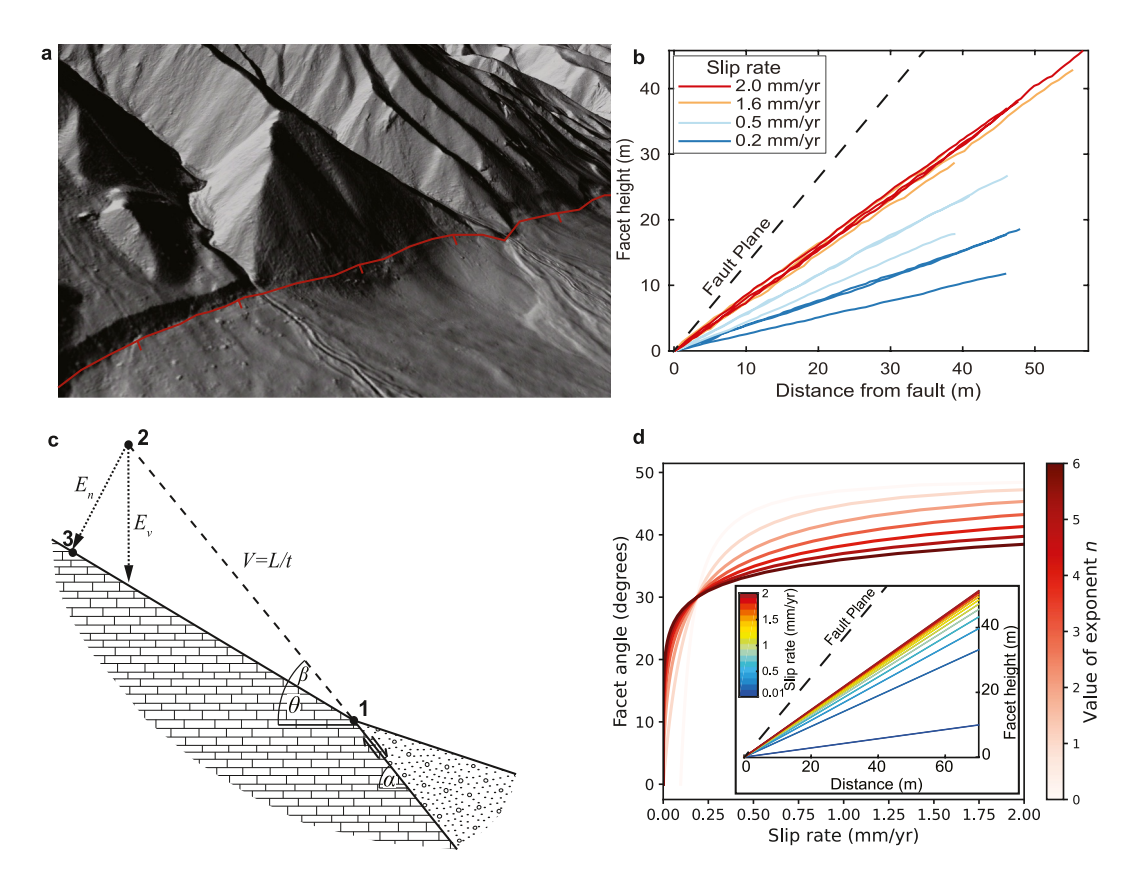


Figure 1. Facet slopes and geometric model of their evolution. (a) Perspective view of shaded relief map showing planar facet slopes above the range-bounding normal fault (red line with ticks on down dropped side), Nephi segment, Wastach fault zone, Utah. Central facet is ~350 m wide across its base. (b) Plot of characteristic facet profiles from the southern half of the Wasatch fault zone. Representative fault plane shown with dashed line. Profiles are colored by Holocene slip rate of local fault segment from (Hatem, Reitman, et al., 2022). Note similarity to theoretical facet profiles shown in inset of panel (d). (c) Schematic illustrating the geometry and proposed evolution of a normal-fault facet slope: α is the fault dip angle, θ is the facet dip angle, and β is the difference between them. L represents the accumulated fault displacement between points 1 and 2, over a time period t. E_n and E_v represent the slope-normal and vertical erosion rate, respectively, at point 3 over the same time period, and V is the fault slip rate assuming pure dip slip. Modified from Tucker et al. (2011, 2020). (d) Plot of theoretical relations of facet dip angle against slip rate (Equation 2) for increasingly nonlinear gradient-erosion rate functions (Equation 4). Inset: Theoretical facet profiles colored by slip rate assuming n=3 in Equation 4.

dense spatial coverage to map the spatio-temporal evolution of fault zones. This is particularly problematic given the evidence of time-variable strain release and the importance of fault segment boundaries in setting the earthquake hazard emerging from studies on faults with detailed Quaternary slip-rate records (Field et al., 2025; Friedrich et al., 2003; Gold et al., 2013; Kirby et al., 2008; Pérouse & Wernicke, 2017; Smith et al., 2024; Verdecchia et al., 2019).

In this paper, we demonstrate how a complementary method, normal-fault facet-angle analysis, can be used to estimate relative and absolute slip rates, averaged at an intermediate timescale of 10–100 ka, and at high spatial resolution, along normal fault arrays hundreds of kilometers long. Specifically, when applied to the Wasatch fault zone (WFZ), we find marked variation in slip rate between the central segments and distal ones, well-defined segment boundaries on distal segments but not on the central segments, as well as evidence of slip rate acceleration in the Holocene.

Triangular facets (also known as faceted spurs, facet slopes, or facets), which rise prominently above fault traces, are striking, nearly planer landforms associated with active extensional provinces (Figures 1a and 1b, Figure S1 in Supporting Information S1; Cotton, 1950; Leeder & Jackson, 1993). Although facet slopes resemble exhumed fault planes, they are modified by erosion as they emerge from below ground, and therefore are less steep than the fault planes from which they arise, typically by tens of degrees (e.g., Figure 1b and Figure S1 in Supporting

STRUBLE ET AL. 2 of 13

Information S1; Armijo et al., 1986; Blackwelder, 1928; Cotton, 1950; Gilluly, 1928; Tucker et al., 2011, 2020; Wallace, 1978).

In theory, facet surfaces that originate from progressive slip along a steeply dipping fault and are exposed to hillslope-erosion processes should record the balance between the fault slip that creates the facet and erosion that destroys it. Owing to the potential to use topographic form as a fault slip-rate proxy, the morpho-tectonic development of normal-fault footwalls has been of great interest (Blackwelder, 1928; Davis, 1903; DePolo & Anderson, 2000; Ganas et al., 2005; Gilbert, 1875, 1928; Hamblin, 1976; Rao et al., 2017; Strak et al., 2011; Tesson et al., 2021; Topal et al., 2016; Tsimi & Ganas, 2015; Wallace, 1978; Wilkinson et al., 2015; Zuchiewicz & McCalpin, 2000). Some studies support empirical relations between facet height and fault slip rate (DePolo & Anderson, 2000; Petit, Meyer, et al., 2009; Rao et al., 2017; Strak et al., 2011; Tsimi & Ganas, 2015), but the timedependent nature of facet height (Hergarten, 2024) and uncertainty regarding timescales to reach a steady height have limited broad application of these relations. Other studies have shown through empirical correlation (Topal et al., 2016; Tsimi & Ganas, 2015), numerical and physical landscape evolution modeling (Hergarten, 2024; Petit, Gunnell, et al., 2009; Strak et al., 2011; Tucker et al., 2020), or through the observation of systematic increases in facet inclination (Menges, 1990) moving from slowly slipping fault tips to the more rapidly slipping fault center (Cowie & Roberts, 2001; Dawers et al., 1993; Roberts & Michetti, 2004; Scholz & Lawler, 2004; Willemse et al., 1996), that facet inclination reflects fault slip rate. These studies have provided insight into the morphotectonics of facet slopes, but no general theory of facet evolution has emerged to extract slip rate from the global distribution of normal-fault bounded ranges that have different fault dips and facet erosion rates.

2. Geometric Model of Facet Evolution: Predictions and Practice

To combine general elements of normal-fault facet evolution, Tucker et al. (2011, 2020) suggested the following geometric model (Figure 1c). After a fault scarp forms during an earthquake, it begins to erode. As fault slip continues to accumulate at a slip rate, V, a point on this fault scarp will be translated upward in the direction of the slip vector a distance L (Figure 1c, point 1 to point 2). During the same time interval, t, the facet surface will continue to undergo weathering and erosion to be worn back by a corresponding slope-normal erosion rate, E_n (Figure 1c, point 2 to point 3). If the slope-normal erosion rate is relatively uniform on the facet and steady in time, this combination of progressive fault slip and erosion gives rise to planar facet profiles that are less steep than the fault plane (Figure 1 and Figure S1 in Supporting Information S1). The difference in angle between fault dip, α , and facet dip, θ , angle β , is given by

$$\sin \beta = \sin(\alpha - \theta) = \frac{E_n}{V},\tag{1}$$

which can then be rearranged as an explicit equation for facet dip angle

$$\theta = \alpha - \sin^{-1}\left(\frac{E_n}{V}\right),\tag{2}$$

or slip rate

$$V = \frac{E_n}{\sin(\alpha - \theta)}. (3)$$

This simple theoretical relation is consistent with process-based numerical models of facet slope evolution, with the proviso that E_n and E_v are expected to vary systematically with slope angle, climate, and lithology (Hergarten, 2024; Tucker et al., 2011, 2020).

In the absence of direct erosion rate estimates for each facet, estimating the relative slip rate along strike of a normal fault with Equation 3, requires knowledge of how the erosion rate scales with the facet dip angle. For slopes steeper than 10° or 20° , a combination of field, experimental, and theoretical work indicates that sediment flux on a quasi-steady hillslope, and hence the slope-averaged erosion rate, is not a simple linear function of slope gradient, S (i.e., $S = \tan \theta$). Rather, erosion rate increases more than linearly with gradient (Andrews & Bucknam, 1987; DiBiase et al., 2010; Roering et al., 1999; Tucker et al., 2018, 2020). The exact functional form

STRUBLE ET AL. 3 of 13

remains uncertain, and likely depends on factors such as lithology, soil-cover thickness, and the proportion of bedrock exposed (DiBiase et al., 2018; Johnstone & Hilley, 2015; Neely et al., 2019; Roering, 2008; Tucker et al., 2018). Current hillslope evolution theory suggests that (a) fully soil-mantled slopes have a maximum stable angle (Carson & Petley, 1970; Roering et al., 1999), but (b) as that angle is approached, thinning of the soil can impede transport (Johnstone & Hilley, 2015; Roering, 2008), and finally (c) observations and numerical models of bedrock fault scarps and facets imply that progressive exposure of mechanically strong bedrock can allow slopes to remain much steeper than they would be if they consisted solely of unconsolidated soil or sediment (Tucker et al., 2011, 2020).

Given the present uncertainty about the exact form of the gradient-erosion relation for steep, partly rocky slopes, a simple approach seems warranted. Here, for purposes of basic model exploration and as an initial feasibility test, we apply a power-law gradient-erosion relation of the form

$$E_{v} = kS^{n} = k(\tan \theta)^{n}, \tag{4}$$

in which E_v is the vertical erosion rate ($E_v = E_n/\cos\theta$), k is an erosion coefficient with dimensions of velocity, and n is the power. Using this erosion rate relation, Equation 3 can be written as

$$V = \frac{k(\tan \theta)^n \cos \theta}{\sin(\alpha - \theta)}.$$
 (5)

Tucker et al. (2020) showed that nearly planer facet slopes, as opposed to highly convex-up slopes, were the resulting form of facet longitudinal profiles across a wide range of erosion, weathering, and slip rates. On planar slopes, simple relations, like Equation 4, that lack dependence on upslope area are a natural choice (Hergarten, 2024). Furthermore, current models of sediment flux and erosion on steep slopes commonly imply a hyper-linear relation between erosion rate and slope gradient. For example, Ganti et al. (2012) showed that a cubic form results from Taylor expansion around the popular Andrews-Bucknam transport law for steep slopes. Similarly, when using parameters representative of facet slopes, the nonlinear hillslope transport equation of Roering et al. (1999) produces a similar S - E curve as Equation 4 with $n \sim 3$ (Figure S2 in Supporting Information S1). As such, we explore a range of potential n values around n = 3, ranging from one to six.

For increasing values of *n*, the geometric model predicts that facet inclination is a monotonic but increasingly nonlinear function of slip rate (Figure 1d). Thus, an expected consequence of a nonlinear erosion rate-gradient relation is that above a certain slip rate, facet inclination increases only slightly with further increases in slip rate. In other words, facet dip angle will most sensitively record changes in fault slip rate at low to moderate slip rates, whereas at high slip rates, changes in facet dip angle will be muted.

Similarly, uncertainty in the form of the erosion relation inevitably introduces uncertainty into absolute slip-rate estimates from Equation 5. In principle, however, one could substitute any viable alternative relation for E_{ν} in Equation 3, given adequate constraints on its parameters (such as threshold angle or effective soil thickness). Alternatively, as demonstrated below, the needed constraint on millennial-scale erosion rates could be obtained directly through cosmogenic-radionuclide analysis on specific facets of interest.

As detailed in the methods section, applying this model requires well-developed facet slopes in the footwall for which baselevel is controlled by a single range-bounding normal fault. Erosion on facets should be by disturbance-driven creep processes, rather than by large-scale landsliding for which bedrock strength determines slope inclination. It has been shown that if deep-seated bedrock landslides dominate mass movement, facet angles can be uniform along strike of the fault, independent of slip rate, and equal to the threshold slope angle set by bedrock strength (Densmore et al., 1998, 2004; Ellis et al., 1999; Strak et al., 2011). Finally, fault-block rotation must play relatively little role in setting the difference between facet and fault-plane inclination on length scales of a \sim 100 m and time scales \sim 100 ka.

Where the above conditions are met, Equations 2 and 3 provide a testable prediction: along a fault array, one should observe a correlation between facet angle and fault slip rate, such that facet dip angle provides a qualitative proxy for slip rate. Moreover, where estimates of long-term erosion rate on individual facets are available, it should be possible to estimate the absolute slip rate, given the dip angle of the fault, α , and of the facet above it, θ , (Equation 3). In this paper, we test these predictions along the WFZ.

STRUBLE ET AL. 4 of 13

3. Wasatch Fault Zone as a Test Case for Facet-Angle Analysis

The WFZ, which runs from southern Idaho to central Utah, USA, and defines the eastern boundary of the Basin and Range extensional province (Figure 2), is one of the longest, most active normal faults in the United States. Detailed geologic, thermochronologic, geodedic, and paleoseismic studies have yielded slip rate estimates over timescales ranging from millions to tens of years for all 10 of the primary fault segments (Armstrong et al., 2004; Ehlers et al., 2003; Friedrich et al., 2003; Hatem, Reitman, et al., 2022; Johnson et al., 2024; McCalpin & Nishenko, 1996; Schwartz & Coppersmith, 1984; Smith et al., 2024; Swan et al., 1980; Valentini et al., 2019; Wong et al., 2016).

The WFZ is a structurally mature, segmented fault array with total throw on the central segments estimated at over 10 km (Parry & Bruhn, 1986, 1987). Fault dip angle has been measured from well-preserved bedrock fault scarps at the foot of the range (e.g., Figure S1 in Supporting Information S1), structural data, geophysical techniques, source seismology, and inversion of geodetic data (Bruhn et al., 1987; Chang et al., 2006; Collettini & Sibson, 2001; Wong et al., 2016; Zoback, 1992). Although fault dip varies from place to place, no systematic trends have been reported along strike, such that a single preferred value of $50^{\circ} \pm 15^{\circ}$, has been used in the most recent fault models (Hatem, Collett, et al., 2022; Hatem, Reitman, et al., 2022; Wong et al., 2016).

Vertical slip rates since WFZ initiation in the Middle Miocene are thought to be 0.5–0.7 mm/yr, but these likely slowed in Plio-Quaternary time to 0.2–0.4 mm/yr and had little spatial variation in rate across the five central segments (Nephi, Provo, Salt Lake City, Weber, and Brigham City) (Armstrong et al., 2004; Friedrich et al., 2003). On 100-ka timescales, vertical slip rates on the central WFZ are likely in the range of 0.2–0.6 mm/yr (Friedrich et al., 2003; Smith et al., 2024), whereas Holocene vertical rates are much higher, centered around ~1.5 mm/yr, and in broad agreement with geodetically determined rates (Friedrich et al., 2003; Hatem, Reitman, et al., 2022; Johnson et al., 2024; Wong et al., 2016). Additionally, the spatially dense measurements of Holocene rates reveal a distinct spatial pattern wherein slip rates progressively decrease from ~1.5 mm/yr on the central segments to 0.3–0.05 mm/yr on the end segments (Hatem, Reitman, et al., 2022; Wong et al., 2016) (Figures 2 and 3d). The decline in segment-average slip rate toward the ends of the fault array is broadly consistent with fault theory (Scholz et al., 1993).

4. Methods

To test whether facet dip angle can be used to estimate fault slip rate, we measured facet dip angle along the length of the WFZ, measured millennial-scale erosion rates on facets with in situ cosmogenic ³⁶Cl, and used previous estimates of fault dip (Hatem, Reitman, et al., 2022; Wong et al., 2016) to estimate slip rate. We then compared these facet-derived slip rates with independent estimates of slip rate along the WFZ. Specifically, we tested three hypotheses: (a) that facet angle correlates with slip rate, (b) that relative variations in slip rate along the surface trace of a normal fault can be estimated directly from measurements of facet inclination, and (c) that if facet erosion rate and fault dip are independently known, estimates of absolute fault slip rate on a 10–100 ka timescale can be obtained.

4.1. Measurement of Facet Dip Angle

To select and evaluate a potential facet site, we used a combination of 1 m resolution lidar-derived bare-earth digital elevation model (DEM) hillshades (State of Utah, 2014), geologic maps, and true color high-resolution (\sim 0.5 m) visual satellite imagery accessed via Google Earth. Facets were included in the analysis if they (a) appeared composed of bedrock or bedrock thinly mantled by regolith, but did not appear deeply buried in talus (Figure S3 in Supporting Information S1); (b) were nearly planar and not dissected by concentrated incisional processes that would lead to excessive planform or profile curvature; (c) lacked evidence of deep-seated land-slides; and (d) had baselevel controlled by a single range-bounding normal fault, which removed facets with bases directly adjacent to active channels or wide, complex fault zones.

At acceptable profile sites (Data Sets S2 and S3 from McCoy (2025)), we positioned the base of each profile at the highest elevation marked by either the active fault trace, commonly identified by the top of the Holocene fault scarp, or the highest Pleistocene lacustrine deposits and shorelines. Avoiding features related to Lake Bonneville was required for segments north of the Nephi segment where prominent Provo and Bonneville stage shoreline features obscure facet morphology directly above the active fault trace. We identified the top of the profile with an

STRUBLE ET AL. 5 of 13

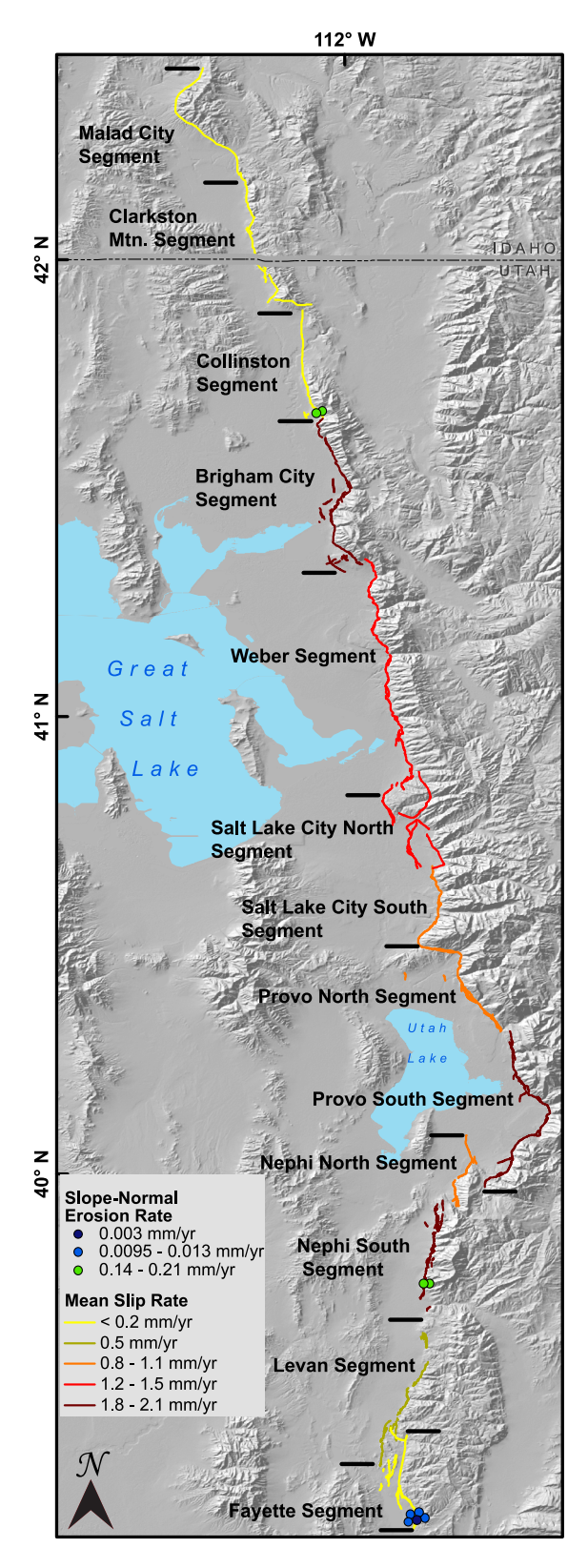


Figure 2.

algorithm that found the highest point in a 100 m search radius centered on the base point. We sampled elevation points along this profile at 1 m spacing to evaluate profile shape. If significant departures from a planar form were found, the facet was discarded, but if a majority of the facet profile was nearly planar (i.e., local slope deviations from the profile average of just a few degrees), the top and bottom points of the profile were adjusted to exclude nonplanar portions. We calculated the mean facet dip angle of the profile by dividing the height of the profile by the horizontal distance of the profile. To quantify the expected variability around this mean angle when moving along a facet profile, we calculated the mean absolute deviation between local slope angles (calculated over increments of 5 m moving along the profile) and the profile mean facet angle. In total, we measured over 500 facet dip angles, with an average distance of \sim 700 m between sites. For plotting measurements, the distance along each individual fault segment (segment endpoints from Quaternary Folds and Faults database (U.S. Geological Survey & Utah Geological Survey, 2017)) was cumulatively summed so that segments with overlap in map view (Figure 2) appear end to end in Figure 3.

4.2. Measurement of Millennial-Scale Erosion Rates Using Cosmogenic $^{36}\mathrm{Cl}$ Data

We estimated millennial-scale erosion rates on representative facet slopes by measuring the concentration of in situ-produced cosmogenic ³⁶Cl in the top 2.5 cm of facet bedrock (Gosse & Phillips, 2001; Granger et al., 2013). In total, we collected and analyzed 9 bedrock samples: 2 from the Collinston segment, 2 from the Nephi segment, and 5 from the Fayette segment (Figure 2). See Text S1 in Supporting Information S1 for complete methods, Figures S4–S7 in Supporting Information S1 for pictures and detailed topographic measurements characterizing each sample location and Data Set S1 (McCoy, 2025) for all inputs used to calculate erosion rates.

We converted the measured concentrations into surface denudation rates using CRONUScalc (Marrero et al., 2016) by assuming steady denudation during sample exhumation through the production zone of ³⁶Cl. We also explored a second potential exhumation history that acknowledges the possibility of a marked deceleration in erosion rate due to regional climate warming in the Holocene, as has been demonstrated for an extensional fault system in central Italy (Tesson et al., 2021; Tucker et al., 2011). In the case of the Wasatch, we do not know whether such a deceleration occurred, but it is plausible given the expanded geographical extent of frost-related hillslope processes across much of North America during the last glacial maximum (Marshall et al., 2021). To provide this second interpretation, we calculated the pre-Holocene erosion rates needed to produce the observed nuclide concentrations if erosion had ceased 10,000 years ago, near the start of the Holocene.

 36 Cl concentrations on the steep facets were low and generally yielded exposure ages of ~ 5 ka (Table S1 in Supporting Information S1), which does not permit this second scenario assuming zero erosion during the Holocene. In

Figure 2. Map of Wasatch fault zone. Fault lines from the Quaternary Fault and Fold Database (U.S. Geological Survey & Utah Geological Survey, 2017) are colored by Holocene vertical slip rates from Hatem, Reitman, et al. (2022) and overlain on a shaded relief map (State of Utah, 2014). Fault segment names and extents are shown in black. Long-term facet erosion rates are shown by colored circles.

STRUBLE ET AL. 6 of 13

contrast, the low-slope samples have enough ³⁶Cl that it is possible to remove 10,000 years worth of ³⁶Cl production and recalculate a faster pre-Holocene rate. However, because these rates were so low to begin with, the second scenario does not yield pre-Holocene erosion rates outside the uncertainty of the first steady-exhumation scenario (estimated as the observed variability in erosion rates on a single facet). Taken together, the two erosion rate scenarios highlight that erosion rates on low-slope facets were likely low both before and during the Holocene, whereas erosion rates on high-slope facets were high in the Holocene, and potentially could have been higher in pre-Holocene times.

4.3. Calculation of 100-ka Average Slip Rate

For facets with erosion rate samples, the measured erosion rates enable direct inference of slip rate using Equation 3. For facets that were not sampled for erosion rates, we used the cosmogenic 36 Cl data to estimate a local slope-dependent erosion rate, by finding the best-fit value of k for n=3 in Equation 4 and then using that relation to calculate slip rate on the basis of facet dip angle (using Equation 5). We propagated uncertainty on α , E_n , and θ through to slip rate estimates using a Monte Carlo approach adapted from Feehan et al. (2023). As described in detail in Text S2 in Supporting Information S1, we assumed that parameter distributions follow uniform distributions between uncertainty bounds, $k \pm 0.037$ mm/yr, $\theta \pm 2.6^{\circ}$ and α in the range of 45° - 65° . We estimated the expected slip rate uncertainty by taking the 5th to the 95th percentile of the cumulative distribution of estimated slip rates produced by the 10,000 Monte Carlo runs for each facet. With a slip rate of ~ 1 mm/yr, 100 m long facet profiles represent facet evolution over a ~ 100 -ka timescale and is the approximate timescale over which slip rates derived from facet analysis are averaged.

5. Resolving Relative Slip Rates Along Strike

Along the length of the WFZ, we find that mountain-front facet angle varies systematically along strike of the fault zone (Figure 3a). Facet inclination ranges from 5° to over 45° along the entire length of the fault zone. The segment-averaged facet inclination ranges from greater than 35° in the center of the fault zone to $<20^{\circ}$ at the southern end.

Comparison of Figures 3a and 3d, as well as Figure S8 in Supporting Information S1 reveal a positive correlation (Pearson correlation coefficient of 0.61 and *p*-value of 0.027) between facet dip angle and the independently constrained Holocene slip rate (i.e., steep facet slopes are found along central segments where slip rates are high, whereas slowly slipping distal segments have gently dipping facet slopes). Fault dip angle lacks systematic variation along strike (Wong et al., 2016) and thus cannot explain the observed spatial variation in facet dip angles. This result is a positive test of our first hypothesis that variations in slip rate along the fault zone produce corresponding variations in the facet dip angle.

Moving from central segments to distal ones, step changes in facet inclination correspond to previously mapped (Machette et al., 1991; McCalpin & Nishenko, 1996; Schwartz & Coppersmith, 1984; Swan et al., 1980; Verdecchia et al., 2019) fault-segment boundaries (Figure 3a). Furthermore, along individual fault segments near the ends of the WFZ, facet angles are systematically higher near segment centers than at segment tips, which matches the expected slip rate distribution on individual fault segments (Dawers et al., 1993; Roberts & Michetti, 2004; Scholz & Lawler, 2004; Willemse et al., 1996). Along the Levan segment ("Le" in Figure 3a), for example, facets dip $\sim 10^\circ$ at the segment tips, whereas they dip over 30° in the segment center. Similar patterns are less clear, to completely absent, on the central segments (Figure 3a).

Also notable is that segment-averaged facet inclination varies by less than a factor of two along the entire WFZ, whereas Holocene slip rates vary by more than a factor of 10. Much of this variation in facet dip angles can be seen along individual fault segments in the southern WFZ, where slip rates are less than 1 mm/yr. In the higher slip rate central segments only subtle along-strike variation in facet dip angles is observed (compare, e.g., facet angles on segments Le (Levan) and Provo (Pr) in Figure 3a). This decreasing sensitivity of facet inclination at high slip rates is consistent with theory. As the slope dependence of erosion rate becomes increasingly hyper-linear (n > 1), the range of predicted facet inclination decreases for the same range in slip rate (Figure 1d). These results highlight that facet inclination records slip rate best at low to moderate slip rates and loses sensitivity at high slip rates, which for the parameters used here occurs around 0.5 mm/yr.

STRUBLE ET AL. 7 of 13

19448007, 2025, 22, Downloaded

library.wiley.com/doi/10.1029/2025GL117713 by University Of Leeds Brotherton, Wiley Online Library on [25/11/2025]. See the Terms and Conditions

Figure 3. Variation of facet dip angle, erosion rate, and slip rate along the Wastach fault zone. (a) Plot of facet dip angle against distance along strike with vertical error bars showing uncertainty on facet dip angle of $\pm 2.6^{\circ}$. Fault segments labeled as Ma: Malad City; CM: Clarkston Mountain; Co: Collinston; Br: Brigham City; We: Weber; SL_N, SL_S: Salt Lake City north and south; Pr_N, Pr_S: Provo north and south; Ne_N, Ne_S: Nephi north and south; Le: Levan; and Fa: Fayette. Predominant lithology is denoted with colored text as LS: limestone; Meta: metamorphic; SS: sandstone; and MS: mudstone. (b) Measurements of millennial-scale facet erosion rates plotted against facet dip angle. Vertical error bars on individual measurements show analytical uncertainty whereas horizontal error bars show uncertainty on facet dip angle. Large symbols show means of all samples from individual facets. Solid line shows power law fit to the data for n=3, shading shows uncertainty on the best fit power-law coefficient, k. (c) Plot of slip rate against facet inclination from Equation 5. Each of the three lines is for an assumed fault dip of 45° , 55° , or 65° . The empirical relation of Tsimi and Ganas (2015) is shown with a dotted line. (d) Plot of vertical slip rates along the Wasatch fault zone from various sources. See text and legend for details.

STRUBLE ET AL. 8 of 13

To test our third hypothesis about recovering absolute values of slip rate using Equation 3, we first use our measurements of facet dip angle (Figures S5 and S6 in Supporting Information S1), 36 Cl-derived erosion rates (Table S1 in Supporting Information S1), and published values for fault dip (Wong et al., 2016) at the two facets (one from Nephi segment and one from Collinston) that have both erosion rate and independent slip rate measurements. At the Nephi facet where $E_{\nu}=0.09\pm0.02$ mm/yr, $\theta=38.4^{\circ}\pm2.6^{\circ}$ and $\alpha=50^{\circ}_{-5^{\circ}}^{+15^{\circ}}$, Equation 3 yields a slip rate with a vertical component of $0.27^{+0.25}_{-0.09}$ mm/yr (mean and 90% highest density interval). Similarly, on the Collinston facet where $E_{\nu}=0.12\pm0.02$ mm/yr, $\theta=36.7^{\circ}\pm2.6^{\circ}$ and $\alpha=50^{\circ}_{-5^{\circ}}^{+15^{\circ}}$ Equation 3 yields a slip rate with a vertical component of $0.30^{+0.23}_{-0.09}$ mm/yr. Both of these rates compare favorably to rates of 0.2–0.6 mm/yr found over similar 100-ka timescales (a positive test of our hypothesis) but are substantially lower than Holocene slip rates (Figure 3d).

Predicted slip rate from the parameterized Equation 5 emerges as a monotonically increasing, nonlinear function of facet inclination (Figure 3c). The shape of this function contrasts with the linear empirical relation previously proposed (Tsimi & Ganas, 2015) and predicts notably lower slip rates at low to moderate facet angles. Inputting the measured facet angles into the parameterized Equation 5 permits quantitative slip-rate estimates along the entire WFZ (Figure 3d). These facet-derived rates are positively correlated with Holocene rates (Figure S8 in Supporting Information S1, Pearson correlation coefficient of 0.73 and p-value of 0.005). We calculate vertical slip rates of $0.37^{+0.36}_{-0.1}$ mm/yr along the central WFZ, again consistent with independent estimates from geologic and geomorphic features offset over a similar 100-ka timescale, but markedly lower than the Holocene rates (Figure 3).

7. Discussion and Conclusions

We have shown that facet-angle analysis shows promise to estimate relative variation in slip rates along strike of normal faults and, if facet erosion rates are available, estimates of absolute slip rates are possible. This work demonstrates that on suitable normal-fault-bounded range fronts, facet-angle analysis permits efficient constraint of slip rates on 10–100 ka timescales.

Lithology varies along strike of the WFZ, both in type and bedding orientation relative to facet surfaces, but it appears that this lithologic variation exerts only a second-order control on facet inclination. Anomalously steep slopes on the Weber and Brigham City segments do not occur exclusively on lithologies like quartzite or limestone that are commonly most resistant to erosion, and the lowest-angle facets are underlain by resistant limestone. Similarly, on the Levan segment, facet angle changes little between facets underlain by shales and mudstones compared to facets underlain by granitic rocks, and instead varies with the expected slip rate distribution (Figure S9 in Supporting Information S1). Isolated examples can be found, however, for which abrupt changes in lithology appear to explain 5°–10° of anomalously low or high facet angles. On the southern end of the Nephi segment for example, steep facet slopes are underlain by limestone, whereas anomalously gentle slopes appear further north along the segment, where shale interbeds prone to earthflows and deep-seated landslides predominate (Figures S10 and S11 in Supporting Information S1). Thus, although lithology in some cases influences local facet angles, and likely contributes to much of the noise observed in facet-angle measurements (Figure 3a), in total, lithology appears to have a second-order influence on the overall pattern of facet angle along strike of the WFZ.

Conformity between facet-estimated slip rate and independently constrained slip rate over 100-ka timescales not only provides a test of facet-angle analysis, but provides further evidence of significant Holocene acceleration of fault slip rates along the WFZ. The slip rate of $0.37^{+0.36}_{-0.1}$ mm/yr estimated from facets on the central segments is in the range of slip rates estimated for the last ~5 Ma (Armstrong et al., 2004) as well as the last ~200–100 ka (Friedrich et al., 2003; Smith et al., 2024), but is markedly lower than the Holocene rate of ~1.5 mm/yr (Wong et al., 2016). Such a rapid acceleration points to a transient mechanism for clustered strain release (Friedrich et al., 2003), with stress changes resulting from climate-driven lake-level changes seeming a likely explanation (Hampel & Hetzel, 2006; Smith et al., 2024; Xue et al., 2022). The matching spatial pattern between slip rates derived from facet angles and Holocene slip rates suggests that although the magnitude of slip rate has changed in the Holocene, the spatial pattern of slip has remained steady, as might be expected on a mature, segmented normal

STRUBLE ET AL. 9 of 13

19448007, 2025, 22, Downloaded

fault (Cowie & Roberts, 2001). On the northern three segments, however, a notable breakdown in the spatial correlation is observed. Here, the 100-ka slip rate estimated from facets is up to a factor of six higher, as opposed to lower, than the estimated Holocene slip rate (Figure 3d). Without direct measurements of facet erosion rates on these segments a definitive conclusion is hard to reach, but if the facet-derived slip rates are accurate, the rate of seismic moment release on these northern segments is currently underestimated in geologic deformation models (Hatem, Reitman, et al., 2022; Wong et al., 2016).

Slip rates on a 50–100 ka timescale are critical to constrain transient fault behavior, as we have shown here for the WFZ, or to obtain representative slip rates on slowly slipping faults. We have tested this approach in a well-constrained tectonic environment, but our results suggest that facet analysis could readily be extended to less understood normal fault systems, such as in the Apennines of Italy, areas of Greece and Turkey, the Basin and Range in western North America, the Ordos and Baikal regions in northwest Asia, and the East African Rift. In particular, this method lends itself to constraining slow to moderate slip rates (<1 mm/yr) in moderate to rapidly eroding tectonic settings (>0.1 mm/yr). These are precisely the tectonic environments in which representative slip rates and seismic hazard have proven most difficult to constrain by existing methods.

Conflict of Interest

The authors declare no conflicts of interest relevant to this study.

Data Availability Statement

Data and Python Jupyter notebook associated with this manuscript have been archived in a data release hosted on figshare (McCoy, 2025). The DEM of the Wasatch range is available on OpenTopography (State of Utah, 2014).

References

Anderson, J. G., & Biasi, G. P. (2016). What is the basic assumption for probabilistic seismic hazard assessment? Seismological Research Letters, 87(2A), 323–326. https://doi.org/10.1785/0220150232

Andrews, D., & Bucknam, R. C. (1987). Fitting degradation of shoreline scarps by a nonlinear diffusion model. *Journal of Geophysical Research*, 92(B12), 12857–12867. https://doi.org/10.1029/jb092ib12p12857

Armijo, R., Tapponnier, P., Mercier, J., & Han, T. (1986). Quaternary extension in southern Tibet: Field observations and tectonic implications. Journal of Geophysical Research, 91(14), 13–803. https://doi.org/10.1029/jb091ib14p13803

Armstrong, P. A., Taylor, A. R., & Ehlers, T. A. (2004). Is the Wasatch fault footwall (Utah, United States) segmented over million-year time scales? *Geology*, 32(5), 385–388. https://doi.org/10.1130/g20421.1

Blackwelder, E. (1928). The recognition of fault scarps. The Journal of Geology, 36(4), 289-311. https://doi.org/10.1086/623519

Bruhn, R. L., Gibler, P. R., & Parry, W. T. (1987). Rupture characteristics of normal faults: An example from the Wasatch fault zone. Geological Society, London, Special Publications, 28(1), 337–353. https://doi.org/10.1144/gsl.sp.1987.028.01.21

Carson, M., & Petley, D. (1970). The existence of threshold hillslopes in the denudation of the landscape. *Transactions of the Institute of British Geographers*, (49), 71–95. https://doi.org/10.2307/621642

Chang, W.-L., Smith, R. B., Meertens, C. M., & Harris, R. A. (2006). Contemporary deformation of the Wasatch Fault, Utah, from GPS measurements with implications for interseismic fault behavior and earthquake hazard: Observations and kinematic analysis. *Journal of Geophysical Research*, 111(B11), B11405. https://doi.org/10.1029/2006jb004326

Collettini, C., & Sibson, R. H. (2001). Normal faults, normal friction? Geology, 29(10), 927–930. https://doi.org/10.1130/0091-7613(2001) 029<0927;nfnf>2.0.co;2

Cotton, C. (1950). Tectonic scarps and fault valleys. Geological Society of America Bulletin, 61(7), 717–758. https://doi.org/10.1130/0016-7606 (1950)61[717:tsafv]2.0.co;2

Cowie, P., & Roberts, G. (2001). Constraining slip rates and spacings for active normal faults. *Journal of Structural Geology*, 23(12), 1901–1915. https://doi.org/10.1016/s0191-8141(01)00036-0

Davis, W. M. (1903). The mountain ranges of the great basin. *Harvard University Museum of Comparative Zoology Bulletin*, 40(3), 129–177. Dawers, N., Anders, M., & Scholz, C. (1993). Growth of normal faults: Displacement-length scaling. *Geology*, 21(12), 1107. https://doi.org/10.1130/0091-7613(1993)021<1107:gonfdl>2.3.co;2

Densmore, A. L., Dawers, N., Gupta, S., Guidon, R., & Goldin, T. (2004). Footwall topographic development during continental extension. *Journal of Geophysical Research*, 109(F3), F03001. https://doi.org/10.1029/2003jf000115

Densmore, A. L., Ellis, M. A., & Anderson, R. S. (1998). Landsliding and the evolution of normal-fault-bounded mountains. *Journal of Geophysical Research*, 103(B7), 15203–15219. https://doi.org/10.1029/98jb00510

DePolo, C., & Anderson, J. (2000). Estimating the slip rates of normal faults in the great basin, USA. Basin Research, 12(3-4), 227-240. https://doi.org/10.1111/j.1365-2117.2000.00131.x

DiBiase, R. A., Rossi, M. W., & Neely, A. B. (2018). Fracture density and grain size controls on the relief structure of bedrock landscapes. *Geology*, 46(5), 399–402. https://doi.org/10.1130/g40006.1

DiBiase, R. A., Whipple, K., Heimsath, A., & Ouimet, W. (2010). Landscape form and millennial erosion rates in the San Gabriel Mountains, CA. Earth and Planetary Science Letters, 289(1–2), 134–144. https://doi.org/10.1016/j.epsl.2009.10.036

Ehlers, T. A., Willett, S. D., Armstrong, P. A., & Chapman, D. S. (2003). Exhumation of the central Wasatch Mountains, Utah: 2. Thermokinematic model of exhumation, erosion, and thermochronometer interpretation. *Journal of Geophysical Research*, 108(B3), 2173. https://doi.org/10.1029/2001jb001723

Acknowledgments

This research was supported by the US National Science Foundation (EAR-1349390 and EAR-2100702). We thank Editor Germán Prieto, and reviewers Chelsea Scott and George Hilley for comments that helped improve the manuscript.

STRUBLE ET AL. 10 of 13

- Ellis, M., Densmore, A., & Anderson, R. (1999). Development of mountainous topography in the basin ranges, USA. Basin Research, 11(1), 21–42. https://doi.org/10.1046/j.1365-2117.1999.00087.x
- Feehan, S. A., McCoy, S. W., Scheingross, J. S., & Gardner, M. H. (2023). Quantifying variability of incipient-motion thresholds in gravel-bedded Rivers using a grain-scale force-balance model. *Journal of Geophysical Research: Earth Surface*, 128(9), e2023JF007162. https://doi.org/10.1029/2023JF007162
- Field, E. H., Hatem, A. E., Shaw, B. E., Page, M. T., Mai, P. M., Milner, K. R., et al. (2025). A scientific vision and roadmap for earthquake rupture forecast developments, A USGS perspective. *Bulletin of the Seismological Society of America*. https://doi.org/10.1785/0120240217
- Friedrich, A., Wernicke, B., Niemi, N., Bennett, R., & Davis, J. (2003). Comparison of geodetic and geologic data from the Wasatch region, Utah, and implications for the spectral character of Earth deformation at periods of 10 to 10 million years. *Journal of Geophysical Research*, 108(4), 2199. https://doi.org/10.1029/2001jb000682
- Ganas, A., Pavlides, S., & Karastathis, V. (2005). DEM-based morphometry of range-front escarpments in Attica, central Greece, and its relation to fault slip rates. *Geomorphology*, 65(3–4), 301–319. https://doi.org/10.1016/j.geomorph.2004.09.006
- Ganti, V., Passalacqua, P., & Foufoula-Georgiou, E. (2012). A sub-grid scale closure for nonlinear hillslope sediment transport models. *Journal of Geophysical Research*, 117(F2), F02012. https://doi.org/10.1029/2011jf002181
- Gilbert, G. (1875). Report on the geology of portions of Nevada, Utah, California, and Arizona (Vol. 3). US Geographical and Geological Survey. Gilbert, G. (1928). Studies of basin-range structure (Vol. 153). United States Government Printing Office.
- Gilluly, J. (1928). Basin range faulting along the Oquirrh range, Utah. Bulletin of the Geological Society of America, 39(4), 1103–1130. https://doi.org/10.1130/gsab-39-1103
- Gold, R., dePolo, C., Briggs, R., Crone, A., & Gosse, J. (2013). Late Quaternary slip-rate variations along the warm springs valley fault system, northern walker Lane, California–Nevada border. *Bulletin of the Seismological Society of America*, 103(1), 542–558. https://doi.org/10.1785/0120120020
- Gosse, J. C., & Phillips, F. M. (2001). Terrestrial in situ cosmogenic nuclides: Theory and application. *Quaternary Science Reviews*, 20(14), 1475–1560. https://doi.org/10.1016/S0277-3791(00)00171-2
- Granger, D. E., Lifton, N. A., & Willenbring, J. K. (2013). A cosmic trip: 25 years of cosmogenic nuclides in geology. Geological Society of America Bulletin, 125(9–10), 1379–1402. https://doi.org/10.1130/B30774.1
- Hamblin, W. (1976). Patterns of displacement along the Wasatch fault. Geology, 4(10), 619. https://doi.org/10.1130/0091-7613(1976)4<619: podatw>2.0.co;2
- Hampel, A., & Hetzel, R. (2006). Response of normal faults to glacial-interglacial fluctuations of ice and water masses on Earth's surface. *Journal of Geophysical Research*, 111(B6), B06406. https://doi.org/10.1029/2005JB004124
- Hatem, A. E., Collett, C. M., Briggs, R. W., Gold, R. D., Angster, S. J., Field, E. H., et al. (2022). Simplifying complex fault data for systems-level analysis: Earthquake geology inputs for U.S. NSHM 2023. Scientific Data, 9(1), 506. https://doi.org/10.1038/s41597-022-01609-7
- Hatem, A. E., Reitman, N. G., Briggs, R. W., Gold, R. D., Thompson Jobe, J. A., & Burgette, R. J. (2022). Western U.S. geologic deformation model for use in the U.S. National Seismic Hazard model 2023. Seismological Research Letters, 93(6), 3053–3067. https://doi.org/10.1785/
- Hergarten, S. (2024). A simple model for faceted topographies at normal faults based on an extended stream-power law. *Earth Surface Dynamics*, 12(6), 1315–1327. https://doi.org/10.5194/esurf-12-1315-2024
- Johnson, K. M., Hammond, W. C., & Weldon, R. J. II. (2024). Review of geodetic and geologic deformation models for 2023 U.S. national seismic hazard model. Bulletin of the Seismological Society of America, 114(3), 1407–1436. https://doi.org/10.1785/0120230137
- Johnstone, S. A., & Hilley, G. E. (2015). Lithologic control on the form of soil-mantled hillslopes. *Geology*, 43(1), 83–86. https://doi.org/10.1130/g36052.1
- Kirby, E., Anandakrishnan, S., Phillips, F., & Marrero, S. (2008). Late Pleistocene slip rate along the Owens Valley fault, eastern California. Geophysical Research Letters, 35(1), L01304. https://doi.org/10.1029/2007gl031970
- Koehler, R. D., & Wesnousky, S. G. (2011). Late Pleistocene regional extension rate derived from earthquake geology of late quaternary faults across the great basin, Nevada, between 38.5 N and 40 N latitude. Geological Society of America Bulletin, 123(3-4), 631-650. https://doi.org/10.1130/B30111.1
- Leeder, M., & Jackson, J. (1993). The interaction between normal faulting and drainage in active extensional basins, with examples from the western United States and central Greece. *Basin Research*, 5(2), 79–102. https://doi.org/10.1111/j.1365-2117.1993.tb00059.x
- Machette, M., Personius, S., Nelson, A., Schwartz, D., & Lund, W. (1991). The Wasatch fault zone, Utah–segmentation and history of Holocene earthquakes. *Journal of Structural Geology*, *13*(2), 137–149. https://doi.org/10.1016/0191-8141(91)90062-n
- Marrero, S. M., Phillips, F. M., Borchers, B., Lifton, N., Aumer, R., & Balco, G. (2016). Cosmogenic nuclide systematics and the CRONUScalc program. *Quaternary Geochronology*, 31, 160–187. https://doi.org/10.1016/j.quageo.2015.09.005
- Marshall, J., Roering, J., Rempel, A., Shafer, S., & Bartlein, P. (2021). Extensive frost weathering across unglaciated North America during the last glacial maximum. *Geophysical Research Letters*, 48(5), e2020GL090305. https://doi.org/10.1029/2020gl090305
- McCalpin, J. (2009). Paleoseismology (Vol. 95). Academic Press.
- McCalpin, J., & Nishenko, S. (1996). Holocene paleoseismicity, temporal clustering, and probabilities of future large (M>7) earthquakes on the Wasatch fault zone, Utah. *Journal of Geophysical Research*, 101(B3), 6233–6253. https://doi.org/10.1029/95jb02851
- McCoy, S. W. (2025). Data sets and code associated with manuscript "Dip Angles of Mountain-Front Facets Encode Long-Term Slip Rate Along the Wasatch Normal Fault, USA". figshare. https://doi.org/10.6084/m9.figshare.29361623.v1
- Menges, C. (1990). Soils and geomorphic evolution of bedrock facets on a tectonically active mountain front, western Sangre de Cristo Mountains, New Mexico. Geomorphology, 3(3–4), 301–332. https://doi.org/10.1016/0169-555x(90)90009-f
- Neely, A. B., DiBiase, R. A., Corbett, L. B., Bierman, P. R., & Caffee, M. W. (2019). Bedrock fracture density controls on hillslope erodibility in steep, rocky landscapes with patchy soil cover, southern California, USA. Earth and Planetary Science Letters, 522, 186–197. https://doi.org/ 10.1016/j.epsl.2019.06.011
- Parry, W., & Bruhn, R. (1986). Pore fluid and seismogenic characteristics of fault rock at depth on the Wasatch fault, Utah. *Journal of Geophysical Research*, 91(B1), 730–744. https://doi.org/10.1029/jb091ib01p00730
- Parry, W., & Bruhn, R. (1987). Fluid inclusion evidence for minimum 11 km vertical offset on the Wasatch fault, Utah. Geology, 15(1), 67–70. https://doi.org/10.1130/0091-7613(1987)15<67:fiefmk>2.0.co;2
- Pérouse, E., & Wernicke, B. P. (2017). Spatiotemporal evolution of fault slip rates in deforming continents: The case of the great basin region, northern basin and range province. *Geosphere*, 13(1), 112–135. https://doi.org/10.1130/ges01295.1
- Petersen, M. D., Moschetti, M. P., Powers, P. M., Mueller, C. S., Haller, K. M., Frankel, A. D., et al. (2015). The 2014 United States national seismic hazard model. *Earthquake Spectra*, 31(1_suppl), S1–S30. https://doi.org/10.1193/120814eqs210m

STRUBLE ET AL. 11 of 13

- Petit, C., Gunnell, Y., Gonga-Saholiariliva, N., Meyer, B., & Seguinot, J. (2009). Faceted spurs at normal fault scarps: Insights from numerical modeling. *Journal of Geophysical Research*, 114(B5), B05403. https://doi.org/10.1029/2008JB005955
- Petit, C., Meyer, B., Gunnell, Y., Jolivet, M., San'kov, V., Strak, V., & Gonga-Saholiariliva, N. (2009). Height of faceted spurs, a proxy for determining long-term throw rates on normal faults: Evidence from the North Baikal Rift System, Siberia. *Tectonics*, 28(6), TC6010. https:// doi.org/10.1029/2009TC002555
- Rao, G., Cheng, Y., Yu, Y., Yan, B., & Lin, A. (2017). Tectonic characteristics of the Lishan piedmont fault in the SE Weihe Graben (central China), as revealed by the geomorphological and structural analyses. *Geomorphology*, 282, 52–63. https://doi.org/10.1016/j.geomorph.2017.
- Roberts, G., & Michetti, A. (2004). Spatial and temporal variations in growth rates along active normal fault systems: An example from the Lazio-Abruzzo Apennines, central Italy. *Journal of Structural Geology*, 26(2), 339–376. https://doi.org/10.1016/s0191-8141(03)00103-2
- Roering, J. (2008). How well can hillslope evolution models "explain" topography? Simulating soil transport and production with high-resolution topographic data. *Geological Society of America Bulletin*, 120(9–10), 1248–1262. https://doi.org/10.1130/B26283.1
- Roering, J., Kirchner, J., & Dietrich, W. (1999). Evidence for nonlinear, diffusive sediment transport on hillslopes and implications for landscape morphology. Water Resources Research, 35(3), 853–870. https://doi.org/10.1029/1998WR900090
- Scholz, C. H., Dawers, N., Yu, J.-Z., Anders, M., & Cowie, P. (1993). Fault growth and fault scaling laws: Preliminary results. *Journal of Geophysical Research*, 98(B12), 21951–21961. https://doi.org/10.1029/93jb01008
- Scholz, C. H., & Lawler, T. M. (2004). Slip tapers at the tips of faults and earthquake ruptures. Geophysical Research Letters, 31(21), L21609. https://doi.org/10.1029/2004g1021030
- Schwartz, D., & Coppersmith, K. (1984). Fault behavior and characteristic earthquakes: Examples from the Wasatch and San Andreas fault zones. Journal of Geophysical Research, 89(B7), 5681–5698. https://doi.org/10.1029/jb089ib07p05681
- Smith, A. G. G., Fox, M., Moore, J. R., Miller, S. R., Goren, L., Morriss, M. C., & Carter, A. (2024). One million years of climate-driven rock uplift rate variation on the Wasatch fault revealed by fluvial topography. *American Journal of Science*, 324. https://doi.org/10.2475/001c.92194
- State of Utah. (2014). State of Utah acquired LiDAR data Wasatch front. *Distributed by OpenTopography*. https://doi.org/10.5069/G9TH8JNQ Strak, V., Dominguez, S., Petit, C., Meyer, B., & Loget, N. (2011). Interaction between normal fault slip and erosion on relief evolution: Insights from experimental modelling. *Tectonophysics*. 513(1–4), 1–19. https://doi.org/10.1016/j.tecto.2011.10.005
- Swan, F., Schwartz, D., & Cluff, L. (1980). Recurrence of moderate to large magnitude earthquakes produced by surface faulting on the Wasatch fault zone, Utah. *Bulletin of the Seismological Society of America*, 70(5), 1431–1462.
- Tesson, J., Benedetti, L., Godard, V., Novaes, C., Fleury, J., & Team, A. (2021). Slip rate determined from cosmogenic nuclides on normal-fault facets. *Geology*, 49(1), 66–70. https://doi.org/10.1130/g47644.1
- Topal, S., Keller, E., Bufe, A., & Koçyiğit, A. (2016). Tectonic geomorphology of a large normal fault: Akşehir fault, SW Turkey. Geomorphology, 259, 55–69. https://doi.org/10.1016/j.geomorph.2016.01.014
- Tsimi, C., & Ganas, A. (2015). Using the aster global Dem to derive empirical relationships among triangular facet slope, facet height and slip
- rates along active normal faults. *Geomorphology*, 234, 171–181. https://doi.org/10.1016/j.geomorph.2015.01.018

 Tucker, G. E., Hobley, D., McCoy, S. W., & Struble, W. T. (2020). Modeling the shape and evolution of normal-fault facets. *Journal of*
- Geophysical Research: Earth Surface, 125(3), e2019JF005305. https://doi.org/10.1029/2019JF005305

 Tucker, G. E., McCoy, S., Whittaker, A., Roberts, G., Lancaster, S., & Phillips, R. (2011). Geomorphic significance of postglacial bedrock scarps on normal-fault footwalls. Journal of Geophysical Research, 116(F1), F01022. https://doi.org/10.1029/2010JF001861
- Tucker, G. E., McCoy, S. W., & Hobley, D. E. (2018). A lattice grain model of hillslope evolution. *Earth Surface Dynamics*, 6(3), 563–582. https://doi.org/10.5194/esurf-6-563-2018
- U.S. Geological Survey, & Utah Geological Survey. (2017). Quaternary fault and fold database for the United States. Retrieved from https://www.usgs.gov/natural-hazards/earthouake-hazards/faults
- Valentini, A., DuRoss, C. B., Field, E. H., Gold, R. D., Briggs, R. W., Visini, F., & Pace, B. (2019). Relaxing segmentation on the Wasatch fault zone: Impact on seismic hazard. Bulletin of the Seismological Society of America, 110(1), 83–109. https://doi.org/10.1785/0120190088
- Verdecchia, A., Carena, S., Pace, B., & DuRoss, C. B. (2019). The effect of stress changes on time-dependent earthquake probabilities for the central Wasatch fault zone, Utah, USA. *Geophysical Journal International*, 219(2), ggz336. https://doi.org/10.1093/gji/ggz336
- Wallace, R. (1978). Geometry and rates of change of fault-generated range fronts, north-central Nevada. Journal of Research of the U. S. Geological Survey, 6(5), 637–650.
- Wesnousky, S. G. (1994). The Gutenberg-Richter or characteristic earthquake distribution, which is it? Bulletin of the Seismological Society of America, 84(6), 1940–1959. https://doi.org/10.1785/bssa0840061940
- Wesnousky, S. G., Barron, A. D., Briggs, R. W., Caskey, S. J., Kumar, S., & Owen, L. (2005). Paleoseismic transect across the northern great basin. *Journal of Geophysical Research*, 110(B5), B05408. https://doi.org/10.1029/2004JB003283
- Wilkinson, M., Roberts, G. P., McCaffrey, K., Cowie, P. A., Walker, J. P. F., Papanikolaou, I., et al. (2015). Slip distributions on active normal faults measured from LiDAR and field mapping of geomorphic offsets: An example from L'Aquila, Italy, and implications for modelling seismic moment release. *Geomorphology*, 237, 130–141. https://doi.org/10.1016/j.geomorph.2014.04.026
- Willemse, E. J., Pollard, D. D., & Aydin, A. (1996). Three-dimensional analyses of slip distributions on normal fault arrays with consequences for fault scaling. *Journal of Structural Geology*, 18(2–3), 295–309. https://doi.org/10.1016/s0191-8141(96)80051-4
- Woessner, J., Laurentiu, D., Giardini, D., Crowley, H., Cotton, F., Grünthal, G., et al. (2015). The 2013 European seismic hazard model: Key components and results. *Bulletin of Earthquake Engineering*, 13(12), 3553–3596. https://doi.org/10.1007/s10518-015-9795-1
- Wong, I. G., Lund, W. R., Duross, C., Thomas, P., Arabasz, W., Crone, A. J., et al. (2016). Earthquake probabilities for the Wasatch Front region in Utah, Idaho, and Wyoming (Tech. Rep.). *Utah Geological Survey*.
- Xue, L., Moucha, R., & Scholz, C. A. (2022). Climate-driven stress changes and normal fault behavior in the Lake Malawi (Nyasa) rift, East Africa. Earth and Planetary Science Letters, 593, 117693. https://doi.org/10.1016/j.epsl.2022.117693
- Zoback, M. L. C. (1992). Superimposed late Cenozoic, Mesozoic, and possible Proterozoic deformation along the Wasatch fault zone in central Utah (No. 1500–E). U.S. Geological Survey.
- Zuchiewicz, W. A., & McCalpin, J. P. (2000). Geometry of faceted spurs on an active normal fault: Case study of the Central Wasatch fault, Utah, USA. In *Annales societatis geologorum poloniae* (Vol. 70, pp. 231–249).

References From the Supporting Information

Dunne, J., Elmore, D., & Muzikar, P. (1999). Scaling factors for the rates of production of cosmogenic nuclides for geometric shielding and attenuation at depth on sloped surfaces. *Geomorphology*, 27(1), 3–11. https://doi.org/10.1016/s0169-555x(98)00086-5

STRUBLE ET AL. 12 of 13



Geophysical Research Letters

10.1029/2025GL117713

Lifton, N., Sato, T., & Dunai, T. J. (2014). Scaling in situ cosmogenic nuclide production rates using analytical approximations to atmospheric cosmic-ray fluxes. Earth and Planetary Science Letters, 386, 149–160. https://doi.org/10.1016/j.epsl.2013.10.052

Roering, J., Perron, J., & Kirchner, J. (2007). Functional relationships between denudation and hillslope form and relief. Earth and Planetary Science Letters, 264(1), 245–258. https://doi.org/10.1016/j.epsl.2007.09.035

Schwanghart, W., & Scherler, D. (2014). Short communication: TopoToolbox 2 – MATLAB-based software for topographic analysis and modeling in Earth surface sciences. Earth Surface Dynamics, 2(1), 1–7. https://doi.org/10.5194/esurf-2-1-2014

STRUBLE ET AL. 13 of 13